MODIS-Derived Spatially Complete Surface Albedo Products: Spatial and Temporal Pixel Distribution and Zonal Averages

ERIC G. MOODY,* MICHAEL D. KING,+ CRYSTAL B. SCHAAF,# AND STEVEN PLATNICK+

**RS Information Systems, Inc., Lanham, Maryland*
+Earth Sciences Division, NASA Goddard Space Flight Center, Greenbelt, Maryland
#Center for Remote Sensing, Department of Geography, Boston University, Boston, Massachusetts

Journal of Applied Meteorology and Climatology

(Manuscript submitted 21 May 2007, revised 30 November 2007 and 12 February 2008)

Corresponding author address: Eric G. Moody, RS Information Systems, Inc., Lanham, MD 20706 USA.

E-mail: eric.g.moody@gmail.com.

ABSTRACT

Five years (2000-2004) of spatially complete snow-free land surface albedo data have been produced using high-quality flagged diffuse bihemispherical (white-sky) and direct-beam directional hemispherical (black-sky) land surface albedo data derived from observations taken by the MODIS instrument aboard NASA's Terra satellite platform (MOD43B3, collection 4). In addition, a spatially complete snow-free aggregate albedo climatology product was generated. These spatially complete products were prepared using an ecosystem-dependant temporal interpolation technique that retrieves missing data within 3-8% error.

These datasets have already been integrated into research and operational projects that require snow-free land surface albedo. As such, this paper provides details regarding the spatial and temporal distribution of the filled versus original MOD43B3 data. The paper also explores the intra- and interannual variation in the five-year data record and provides a qualitative comparison of zonal averages and annual cycles of the filled versus original MOD43B3 data.

The analyses emphasize the data's inter- and intra-annual variation and show the filled data exhibit qualitatively similar large- and small-scale phenological behavior to the original MOD43B3. These analyses thereby serve to showcase the inherent spectral, spatial, and temporal variability in the MOD43B3 data as well as the ability of the fill technique to preserve these unique regional and pixel-level phenological characteristics.

1. Introduction

Surface albedo represents the ratio of reflected to incoming solar radiation at the earth's surface and is a central element in the determination and partitioning of the surface energy balance components. Surface albedo is also important for remote sensing of clouds (King et al. 1992, 2003, 2004; Platnick et al. 2003) and the determination of aerosol optical properties (Kaufman et al. 1997; King et al. 1999; Hsu et al. 2004) from satellite and airborne platforms, as well as from surface-based sun/sky radiometers (Holben et al. 1998; Dubovik et al. 2000).

Snow-free albedo is especially important for biophysically-based land surface models that compute the exchange of energy, water, momentum, and carbon for various land use categories (Sellers et al. 1996; Ingram et al. 1989; Dirmeyer et al. 1994; Whitlock et al. 1995). Partly in response to this need, validated (Liang et al. 2002; Jin et al. 2003a, 2003b; Wang et al. 2004, Zhang et al. 2007) diffuse bihemispherical (white-sky) and direct-beam directional hemispherical (black-sky) land surface albedo data, known as MOD43B3 (Schaaf et al. 1998), have been derived from observations taken by the Moderate Resolution Imaging Spectroradiometer (MODIS) onboard NASA's Terra (King and Herring 2000) spacecraft. Beginning on February 24, 2000, global values at 1 km spatial resolution were produced every 16 days for the first seven MODIS bands, 0.47 through 2.1 μm, and for three broadband spectral regions, 0.3-0.7, 0.3-5.0, and 0.7-5.0 μm.

However, roughly 30% of the global land surface, on an annual equal-angle basis, is obscured due to persistent and transient cloud cover, while another 20% is obscured due to ephemeral and seasonal snow cover. Accordingly, a regionally consistent phenologically-based temporal interpolation technique was developed to provide spatially complete global snow-free land surface albedo. This phenological technique fills missing, lower-quality flagged, and snow-covered

data from the original MOD43B3 dataset with temporally interpolated best estimates that have an accuracy of 3-8% (see Section 2 and Moody et al. 2005 for details).

Since Moody et al. (2005), the authors have slightly refined the technique (Section 2) and applied it to the five individual years of collection 4 MOD43B3 albedo data spanning 2000-2004. In addition, MOD43B3 data from the same period were aggregated and treated using the same technique to produce a five-year albedo climatology. These datasets have had success and are being used in research and operational projects that require interannually variable and spatially complete ephemeral and seasonal snow-free land surface albedo (Hsu et al. 2004, 2006; Marshak et al. 2006; Matsui et al. 2006; Ramon and Santer 2005; Roy et al. 2006; Tegen et al. 2006; Wen et al. 2006; Yu et al. 2006).

The purpose of this paper is therefore two fold. First it gives users ample details regarding the spatial and temporal distributions of filled versus original MOD43B3 data (Section 3). Second, it builds upon previous analysis (Moody et al. 2005) and presents seasonal albedo maps (Section 4) as well as a qualitative comparison of zonally averaged fields and annual phenological cycles of pixels that have been filled versus pixels flagged as original high-quality MOD43B3 data (Section 5). These analyses showcase the ability of the filling technique to preserve regional and pixel-level spatial, spectral, and temporal features that are inherent in the MOD43B3 data.

2. Collection 4 spatially complete albedo products

Collection 4 MOD43B3 data (2000-2004) were processed using an enhanced version of the interpolation algorithm that was originally detailed in Moody et al. 2005. In brief, this temporal interpolation technique is predicated upon the es-

tablishment of a phenological curve for each pixel. When the phenological behavior of a pixel cannot be confidently determined, additional spatial support is introduced via the concept that within a limited region, pixels representing the same ecosystem species will exhibit similar phenological, or temporal, behavior. Variations in local climate, canopy density and structure, and soil conditions, however, will result in significant pixel-to-pixel differences in the relative magnitudes of the behavioral curves. Therefore in order to maintain these spatial pixel-level variations in a temporal sense, the shape of the extent phenological curves in the near ecosystem region will be coupled with all the temporal data that do exist for that pixel to establish the complete phenological curve for that pixel.

It is imperative to appreciate that this filling technique is not based primarily on land cover classes, but instead relies first and foremost on the establishment of robust temporal or phenological curves at each pixel location. Only as a last resort does the technique rely explicitly on the temporal information of local pixels of the same ecosystem class. This fallback approach is only used for a relatively small number of pixels globally, namely in high latitude ephemeral and seasonal snow impacted regions and tropical persistent cloud regions.

To be more explicit, in these last resort situations, local pixel-level statistics of the same ecosystem class are selectively introduced to enhance spatial fidelity and to provide robust temporal trends. Local-level statistics alone are only used in severely underrepresented circumstances, such as a locality in Cameroon where, due to the persistent clouds, no high quality observations are retrieved for an entire year. Although the fallback approach maintains the unique inter-annual magnitude of each pixel's temporal trend, the inter-annual temporal variability of these pixels may be reduced.

The algorithm for processing the Collection 4 MOD43B3 data was enhanced

by selectively introducing five-year aggregate statistics (in lieu of single year statistics) into the fallback approach. In addition, an updated MODIS International Geosphere-Biosphere Programme (IGBP) ecosystem classification dataset (Friedl et al. 2002), referred to as product MOD12Q1 (data 149, 2001), was employed to provide, among other benefits, improved classification of urban areas.

Processing of year 2000 MOD43B3 data also required special attention as data from the first three of the 23 16-day periods (periods 001, 017, and 033) that comprise a year were unavailable as the *Terra* satellite was not yet operational. As an approximation, the five-year aggregate MOD43B3 data and statistics were substituted directly for these three missing periods.

Lastly, the five-year aggregate of high-quality flagged MOD43B3 data was filled using the interpolation technique to provide a five-year average that can be used as an average year. It should be noted that in Antarctica, only year 2002 data were used when aggregating the 5-year average.

3. Spatial and temporal distributions of filled versus original MOD43B3 data

The processing Quality Assurance (QA) of the spatially complete albedo product is a record of whether a pixel in the original MOD43B3 data was flagged as high quality and was thereby preserved or was filled using the temporal interpolation technique (Moody et al. 2005). With this QA information, the spatial and temporal distributions of filled versus MOD43B3 data can be explored to provide researchers with a general reference of when and where they might expect to be using filled data. It can also provide a sense of where there is better temporal coverage that will in turn provide better phenological information for the interpolation technique. While each wavelength may have its own unique number and location of pixels filled, the variation between wavelengths is minor.

As such, data from the 0.86 μm band are used here to illustrate these distributions.

To provide an overall sense of global yearly temporal coverage, Fig. 1 illustrates the number of 16-day periods that a pixel has maintained its original MOD43B3 data. Fig. 1a, the five-year aggregate climatology, shows dramatic improvements in the overall temporal coverage compared to any single-year data (1b-1f). This is especially true in areas with limited or no coverage (ephemeral and seasonal snow-impacted or cloud-covered areas). This increase in temporal coverage can lead to improved descriptions of phenological behavior. Note again that Antarctica aggregate values were derived solely from year 2002 data.

Figs. 1b-1f illustrate that there is a significant degree of interannual variability in the number and location of high-quality flagged MOD43B3 retrievals. They also show that the single-year products will have limited temporal coverage in persistently cloudy regions (tropics, Southeast Asia, southern India) and the ephemeral and seasonally snow-impacted areas (esp. mid to high latitudes in the Northern Hemisphere) in which the snow-free dormant state is not always observed. In areas with no observations are available during the entire year, statistics from the five-year aggregate climatology are used to replace the single-year statistics in order to boost interpolation performance (see Sec. 2).

Global trends in spatial and temporal distributions of filled versus original MOD43B3 data for the five-year climatology and the five single-year products can be discerned from Figs. 2 through 4. These figures confirm that snow-impacted and seasonally or persistently cloudy areas have the largest number of filled pixels, whereas mid-latitude pixels predominantly retain their originality. The region with the best MOD43B3 data coverage is the 20°S-40°S zone, a belt

containing central and southern Australia, southern Africa, and south-central South America. This is partially due, with the exception of parts of South America and Africa, to this region being comprised of predominantly arid ecosystems (deserts and shrublands). For the aggregate climatology, this area consists of nearly all MOD43B3 data, with as few as a fraction of one percent containing filled pixels.

Unsurprisingly, these figures also demonstrate that for either the 5-year climatology or the single-year data, the beginning and end of the year have the highest overall percentage of filled data due to the impact of ephemeral and seasonal snow. The middle of the year has the lowest percentage of filled data, with the majority of filled data residing in tropical regions. In addition, for any 16-day period, the climatology has, on average, 10-20% more MOD43B3 pixels than any single-year data. On an annual global basis, the climatology has 32% filled data compared to 45-50% filled data for any single-year product.

As for ecosystems, the variability (not shown) in percentage filled is primarily due to climatology and the global distribution of ecosystem classes. It is not surprising to find that arid classes (desert, closed shrubs, permanent snow) require the least amount of filling, whereas classes predominantly in the tropics (evergreen broadleaf forest, wetlands) require the most filling. Of the forest classes, the deciduous broadleaf forest (DBF) has the best coverage, primarily due to the majority of these pixels residing in the 50°N-30°N and 10°S-30°S latitude belts. The aggregate climatology dramatically improves the coverage of classes within the broader 50°N-20°N and 10°S-40°S latitude belts (DBF, cropland, crop mosaic, urban, savanna, grassland, and closed shrubs).

4. Inter- and Intra-Annual Temporal and Spatial Variability

Radiative properties of snow-free surfaces are primarily dependent on the ecosystem, the properties of ground and vegetation canopy, soil condition, and local climatology (Reed et al. 1994; Kaduk and Heimann 1996; Schwartz 1998; Schwartz and Reed 1999; White et al. 1997; Zhang et al. 2003; Penuelas et al. 2004). As such, and as illustrated in Figs. 5-7, spatial and temporal variability in albedo arise from the global distribution of these factors and from seasonally changing climatology and growth conditions (often latitudinally correlated). In particular, vegetative surfaces exhibit defined and often dramatic phenological patterns. They can also exhibit curtailed or extended periods of productive vegetation due to interannual climate variability; when examining Figs. 5-7, it is important to note that the averaging nature of the five-year aggregate does not provide for interannual variability.

It is instructive to begin by examining some trends in the aggregate maps, the left column of Fig. 5. In January (Fig. 5a), the Northern Hemisphere's vegetation is in full decay. Vegetation in Southern North America, Europe, and Asia begin to grow during April (Fig. 5c) and reach full maturity around mid-year (Fig. 5e); grass- and crop-lands in the Northern Hemisphere are especially bright in the near-infrared channel during July. The phenological cycle is completed as vegetation senesces during the later part of the year (Fig. 5g). The opposite trends hold for Southern Hemisphere vegetation over the course of the year.

It is also interesting to note, in the left panels of Fig. 5, the variability in 0.86 μm albedo values for regions (large and small) with the same ecosystem classification. For example, West Central Australia is primarily open shrubland, however varying vegetation types and/or levels of productivity cause the albedos to range between ~0.2 and 0.3. Varying soil conditions in the Sahara Desert cause similar speckled patterns. These local inter-ecosystem variations can be espe-

cially pronounced in highly vegetated areas during growth or senescence states. For example, during April (Fig. 5c) crop- and grass-lands in the Mid-Western United States and Western Europe contain areas that have begun to grow while other local regions have not. This can most readily be seen in Western Europe where the vegetation in the United Kingdom and North Western France have begun to grow even though surrounding regions have not.

One can also observe the movement of the ITCZ in panels on the left of Fig. 5. As the ITCZ moves into a region, its associated rainfall provides conditions suitable for vegetative growth which thereby produces increases in the 0.86 μm albedo. This trend can be seen quite readily as the ITCZ begins the year in Southern Africa, progresses northward through April, is in Central Africa mid-year, and begins to make its way south during the later part of the year.

Interannual variability can be explored by comparing the differences between the five-year aggregate (Fig. 5 a, c, e, and h) and the single-year data (Figs. 5-7). For example, croplands in the Mid-Western United States during 2003 (left panels of Fig. 7) are not as bright as the climatology, which may indicate a delayed growth cycle, or perhaps less productive vegetation; the opposite is true for certain Mid-Western regions the following year (2004, right panels of Fig. 7). Similarly, examinations of Australia show substantial interannual variability.

5. Zonal averages and phenology of filled vs original MOD43B3 data

Even with the substantial variability of pixel-level, local, and regional phenological trends that arise from the factors presented in Section 4, Moody et al. (2005) showed that their phenological interpolation technique could fill missing data within 3-8% accuracy. This was accomplished by withholding existent data and testing the ability of the phenological curve to mimic these data. This overall

error or uncertainty in the filled values is a highly convoluted mixture of various instrument, algorithm, and interpolation errors (e.g. number of observations, quality of MOD43B3 data, quality of the temporal information over the period, inter-annual variability in the number of observations and growth conditions, etc.). Despite this inability to directly propagate and identify sources of uncertainty, users can nevertheless gain an appreciation for the conditions under which the spatially complete product was generated by examining the accompanying processing QA information (described in Section 3).

Unfortunately, further direct error analysis in global sense is not possible as the two data types (high-quality flagged MOD43B3 and filled) are mutually exclusive and collectively exhaustive. In addition, alternative (i.e. non-MODIS) validation databases suffer from the same temporal and spatial coverage issues, namely a lack of observations due to cloud or ephemeral snow coverage during the same periods.

Nonetheless, this paper seeks to build upon the previous error analysis by qualitatively comparing zonal averages and annual cycles of pixels that have been filled versus pixels flagged as high-quality MOD43B3 data. Such an analysis can showcase the ability of the filling technique to preserve pixel-level and regional spatial and temporal behavior that is inherent in the MOD43B3 data. For brevity, the analysis of the spatially complete products will be performed using one single year (2002) and the five-year climatology data. While there are interannual variations between single-year data, analysis of a single-year of data will provide representative trends associated with the other years.

The authors chose to perform the analysis using diffuse bihemispherical (white-sky) albedo as this represents reflectance under conditions of isotropic illumination and thereby excludes angular solar effects. To take into account the

various factors, described in Sec. 4, that cause variability in spatial and phenological behavior, the statistics were computed as ecosystem classification dependent ten-degree latitude zonal averages for every 16-day period. For conciseness and to provide trends over a range of albedo values and spectral characteristics, the authors chose to present statistics for three ecosystem classes (cropland, grassland, and mixed forest) and for three bands (0.47 μm, 0.86 μm, and the shortwave broadband 0.3-5.0 μm). This section will proceed with spatial (5a) and temporal (5b) trend discussions, and by examining divergent trends (5c).

a. Zonal averages of filled versus high-quality flagged MOD43B3 data

Figure 8 compares ten-degree latitudinal zonal averages in the single-year (2002) and the aggregate spatially complete albedo data for a single 16-day period (Day 193, July 12-27). For this time of year, there are few filled pixels in the 10°S-40°S latitude belt; less than 10% filled pixels for single-year processing (2002) and less than 1% for the aggregate climatology. Conversely, the 0°-40°N latitude belts vary (by ecosystem) from roughly 40-90% filled pixels for the single-year processing (2002) and 20-70% filled pixels from the aggregate climatology.

For the selected ecosystems and spectral bands, the filled and MOD43B3 pixels have trends that are qualitatively consistent. In the near-infrared 0.86 μm band, the cropland and mixed forest trends exhibit mature growth in the Northern Hemisphere, and are dormant in the Southern Hemisphere. The peak in the grassland occurs in the 20°N-10°N latitude belt; the grasslands of this region are in full growth as the Intertropical Convergence Zone (ITCZ) brings rain to this region during this time of year.

Some slight divergences between trend lines are observed. Upon further

analysis, detailed in Section 5c, these departures arise when there are limited amounts of one type of data (either filled or MOD43B3). For example, in Fig. 8, some of the grassland MOD43B3 and filled data trends slightly diverge in the tropical to sub-tropical latitudes. This is primarily due to the limited number of filled pixels in this latitude belt. More specifically, in the 20°N-10°N region, filled grassland pixels primarily reside in Africa, whereas MOD43B3 pixels primarily reside in the Americas. These regions have different vegetative types and conditions and thereby albedo values. This situation results in latitudinal mean values that diverge even though detailed comparisons of each region show agreement between MOD43B3 and fill data. Perhaps in a counter-intuitive way, these anomalies actually highlight the inherent spatial and temporal variability in the MOD43B3 data as well the ability of the fill methodology to provide values that preserve unique local, regional, and latitudinal phenology.

b. Phenological (temporal) behavior of filled versus high-quality flagged MOD43B3 data

The phenological (temporal) behavior of the single-year (2002) and aggregate climatology data can most readily be examined by focusing on a single latitude belt; the 50°N-40°N latitude belt was selected as its vegetation exhibits large differences in the mean albedo values of the vegetative mature and senescent states. Fig. 9 shows ten-degree latitudinal mean diffuse bihemispherical (white-sky) albedo, as a function of 16-day time period, for each of the 23 time periods and for three ecosystems.

The temporal trends show that the MOD43B3 and filled data exhibit qualitatively similar behavior, with the maximum vegetative growth and dormant states appearing qualitatively consistent (0.86 μm band best shows the vegetative

trends) for both the single-year and aggregate climatology data. A closer inspection, however, reveals that there are some discrepancies. As detailed in Sec. 5a and further in Sec. 5c, these features arise from small sample sizes of MOD43B3 or filled pixels that are disproportionately distributed across the latitude belt. While this situation impacts the latitudinal means, detailed analyses of local averages show that MOD43B3 and fill pixels have comparable values.

For example, during the dormant stages, grasslands from the 0.86 μm 2002 single-year processed data primarily consist of filled pixels. Examining Fig. 9d, the MOD43B3 pixels' trend in the beginning of the year differs from the filled pixels' trend, with maximum deviation occurring near the 16-day period starting at day 17 (17 Jan). During this period, only 18.7% of the latitude belt's pixels are from original MOD43B3 data.

Upon closer inspection, a near majority (48.1%) of these MOD43B3 pixels reside in a single region located in eastern Asia. This region's dormant state has a white-sky albedo (0.278) that is higher than the spatially representative latitudinal average filled pixel state (0.209). As such, the pixels from this area dominate the statistical computation, resulting in differing mean latitudinal MOD43B3 and filled trends during this time of year. However, averages of this region's fill (0.281) and MOD43B3 (0.278) pixels are comparable. During this same time period, the deviation in the aggregate climatology data (Fig. 9c) is reduced. This is primarily due to there being more MOD43B3 data that are better distributed across the latitude belt. In all, this provides further evidence of the spatial and temporal variability inherent in the MOD43B3 data and the ability of the fill procedure to preserve these variations.

In a reverse situation, for the aggregate climatology's grassland 0.47 μm data, Fig. 9c, the filled and MOD43B3 trends differ between days 161 and 289

(peaking at day 257). During this time the filled pixels represent only a fraction of 1% of the total grassland pixels in this latitude belt. In fact, at the peak deviation, day 257, there are only 4,420 filled pixels, or about 0.25% of the total grassland pixels in the latitude belt. Of these 4,420 filled pixels, 4,263 pixels (96.4%) reside in a single, small region located in central Asia.

This region, however, has a filled pixel average (0.106) that differs substantially from the spatially representative MOD43B3 latitudinal average albedo (0.066). As a result, the mean filled pixel latitudinal trend deviates from the spatially representative MOD43B3 latitudinal trend during this time period. Upon closer inspection of this region, it is apparent that the MOD43B3 mean (0.113) is comparable to the filled value mean (0.106). During this same time period, the deviation in the single-year data (Fig. 9d) is reduced due to there being more fill data that are better distributed across the latitude belt. This provides further evidence of the spatial and temporal variability inherent in the MOD43B3 data and the ability of the fill procedure to preserve these local variations.

In the final analysis, the qualitatively similar MOD43B3 and fill pixel temporal trends showcase the ability of the fill technique to properly represent large scale trends. The deviations in trends, perhaps counter-intuitively, highlight both the inherent spatial and temporal variability in the MOD43B3 data as well the ability of the fill methodology to preserve the unique phenological state of each local and regional area.

c. Influence of disproportionately distributed pixels on latitude belt averages

As seen in Sections 5a and 5b, care must be taken when interpreting latitude belt statistical trends as means can be skewed when contributions from regions within the latitude belt are not proportionally distributed; this scenario fre-

quently occurs when there are relatively small numbers of either MOD43B3 or filled pixels (i.e. winter or summer, see Figs. 2-4). Then again, these occurrences provide the chance to showcase the spatial variability inherent in the MOD43B3 product, and the ability of the fill technique to represent local behavior.

To further explain this concept, within a latitude belt an ecosystem's pixels are typically distributed across several landmasses, each of which has unique climatology, vegetative and ground conditions, and structure. Differences between the conditions of each region result in varying albedo magnitudes (dormant and mature) within the same ecosystem class, as seen in Figs. 5-7. With a sample that is proportionately distributed across a latitude belt, these local variances are dampened and a representative latitude belt mean can be computed. However, when the sample is disproportionately distributed across a latitude belt, region(s) can dominate the mean calculation, resulting in a non-representative latitude belt mean.

Small samples in which a single region is wholly over- or underrepresented can exacerbate this problem. As regions (and pixels) have unique magnitudes (dormant or mature) that can vary substantially, a latitudinal mean computed from such a sample could be substantially different than if it had been computed from a proportionally distributed sample. On a positive note, these cases do provide excellent examples of the inherent MOD43B3 regional and pixel-level spatial and temporal variability. These cases also demonstrate the temporal interpolation technique's ability to preserve these inherent MOD43B3 behaviors.

6. Conclusions

In this paper, we describe refinements in the temporal interpolation technique that address areas of limited observation, namely persistently cloudy

(tropical) and ephemeral and seasonal snow-impacted (high latitude) regions. The refined algorithm is then applied to five years (2000-2004) of collection 4 MOD43B3 data. Also described is the creation of a spatially complete ephemeral and seasonal snow-free five-year aggregate climatology product. For this product, five years (2000-2004) of high-quality flagged MOD43B3 observations were aggregated for each of the annual 23 16-day time periods. The remaining missing values were filled using the refined phenological interpolation technique.

This paper also provides additional details regarding the spatial and temporal distributions of the filled versus original MOD43B3 data. Seasonal albedo maps for the five years and the aggregate product are provided. A qualitative comparison of temporal and spatial trends of data that have been filled versus data flagged as original MOD43B3 values is provided. This study underscores the ability of the filling technique to preserve regional and pixel-level spatial, spectral, and temporal behavior that is inherent in the MOD43B3 data.

Single-year and multi-year climatological digital data from this analysis are available for public download at ftp://modis-atmos.gsfc.nasa.gov.

Acknowledgments

The research reported in this article was supported by the MODIS Science Team under NASA contract 621-30-H4 to Goddard Space Flight Center (EGM, MDK, SP) and NASA contract NAS5-31369 to Boston University (CBS). The authors would like to express their appreciation to Dr. Bernard Pinty, European Commission Joint Research Centre, for insightful suggestions to clarify this work and to Dr. Lahouari Bounoua, NASA Goddard Space Flight Center, for providing valuable insight into modeling community requirements and reviewing the methodologies used in this work.

REFERENCES

Bounoua, L., R. DeFries, G. J. Collatz, P. Sellers, and H. Khan, 2002: Effects of land cover conversion on surface climate. *Climatic Change*, **52**, 29-64.

Dirmeyer, P. A. and J. Shukla, 1994: Albedo as a modulator of climate response to tropical deforestation. *J. Geophys. Res.*, **99**, 20863-20878.

Dubovik O., A. Smirnov, B. N. Holben, M. D. King, Y. J. Kaufman, T. F. Eck, and I. Slutsker, 2000: Accuracy assessments of aerosol optical properties retrieved from AERONET sun and sky-radiance measurements. *J. Geophys. Res.*, **105**, 9791-9806.

Friedl, M. A., D. K. McIver, J. C. F. Hodges, X. Y. Zhang, D. Muchoney, A. H. Strahler, C. E. Woodcock, S. Gopal, A. Schneider, A. Cooper, A. Baccini, F. Gao, and C. B. Schaaf, 2002: Global land cover mapping from MODIS: Algorithms and early results. *Remote Sens. Environ.*, **83**, 287-302.

Holben, B. N., T. F. Eck, I. Slutsker, D. Tanré, J. P. Buis, A. Setzer, E. Vermote, J. A. Reagan, Y. J. Kaufman, T. Nakajima, F. Lavenu, I. Jankowiak, and A. Smirnov, 1998: AERONET—A federated instrument network and data archive for aerosol characterization. *Remote Sens. Environ.*, **66**, 1-16.

Hsu, N. C., S. C. Tsay, M. D. King, and J. R. Herman, 2004: Aerosol retrievals over bright-reflecting source regions. *IEEE Trans. Geosci. Remote Sens.*, **42**, 557-569.

____, S. C. Tsay, and M. D. King, 2006: Deep blue retrievals of Asian aerosol properties during ACE-Asia. *IEEE Trans. Geosci. Remote Sens.*, **44**, 3180-3195.

Ingram, W. J., C. A. Wilson, and J. F. B. Mitchell, 1989: Modeling climate change: An assessment of sea ice and surface albedo feedbacks. *J. Geophys. Res.*, **94**, 8609-8622.

Jin, Y., C. B. Schaaf, F. Gao, X. Li, A. H. Strahler, W. Lucht, and S. Liang, 2003a:

Consistency of MODIS surface bidirectional reflectance distribution function and albedo retrievals: 1. Algorithm performance. *J. Geophys. Res.*, **108** (D5), doi:10.1029/2002JD002803.

____, C. B. Schaaf, C. E. Woodcock, F. Gao, X. Li, A. H. Strahler, W. Lucht, and S. Liang, 2003b: Consistency of MODIS surface bidirectional reflectance distribution function and albedo retrievals: 2. Validation. *J. Geophys. Res.*, **108** (D5), doi:10.1029/2002JD002804.

Kaduk, J. and M. Heimann, 1996: A prognostic phenology scheme for global terrestrial carbon cycle models. *Climate Research*, **6**, 1-19.

Kaufman, Y. J., D. Tanré, L. A. Remer, E. F. Vermote, A. Chu, and B. N. Holben, 1997: Operational remote sensing of tropospheric aerosol over land from EOS moderate resolution imaging Spectroradiometer. *J. Geophys. Res.*, **102**, 17051-17067.

King, M. D. and D. D. Herring, 2000: Monitoring Earth's vital signs. *Sci. Amer.*, **282**, 72-77.

____, Y. J. Kaufman, W. P. Menzel, and D. Tanré, 1992: Remote sensing of cloud, aerosol, and water vapor properties from the Moderate Resolution Imaging Spectrometer (MODIS). *IEEE Trans. Geosci. Remote Sens.*, **30**, 2-27.

____, Y. J. Kaufman, D. Tanré, and T. Nakajima, 1999: Remote sensing of tropospheric aerosols from space: Past, present, and future. *Bull. Amer. Meteor. Soc.*, **80**, 2229-2259.

____, W. P. Menzel, Y. J. Kaufman, D. Tanré, B. C. Gao, S. Platnick, S. A. Ackerman, L. A. Remer, R. Pincus, and P. A. Hubanks, 2003: Cloud and aerosol properties, precipitable water, and profiles of temperature and humidity from MODIS. *IEEE Trans. Geosci. Remote Sens.*, **41**, 442-458.

____, S. Platnick, P. Yang, G. T. Arnold, M. A. Gray, J. C. Riédi, S. A. Ackerman,

and K. N. Liou, 2004: Remote sensing of liquid water and ice cloud optical thickness and effective radius in the arctic: Application of airborne multispectral MAS data. *J. Atmos. Oceanic Technol.*, **21**, 857-875.

Liang, S. L., H. L. Fang, M. Z. Chen, C. J. Shuey, C. Walthall, C. Daughtry, J. Morisette, C. Schaaf, and A. Strahler, 2002: Validating MODIS land surface reflectance and albedo products: Methods and preliminary results. *Remote Sens. Environ.*, **83**, 149-162.

Marshak, A., S. Platnick, T. Varnai, G. Wen, and R. F. Cahalan, 2006: Impact of three-dimensional radiative effects on satellite retrievals of cloud droplet sizes. *J. Geophys. Res.*, 111, D09207, doi:10.1029/2005JD006686.

Matsui, T., A. Betran-Przekurat, R. A. Pielke Sr., D. Niyogi, and M. Coughenour, 2006: Continental-scale multi-observation calibration and assessment of Colorado State University Land Model. Part I: Surface albedo. *J. Geophys. Res.*, conditionally accepted.

Moody, E. G., M. D. King, S., Platnick, C. B. Schaaf, and F. Gao, 2005: Spatially complete global spectral surface albedos: Value-added datasets derived from Terra MODIS land products. *IEEE Trans. Geosci. Remote Sens.*, **43**, 144–158.

Penuelas, J., I. Filella, X. Zhang, L. Llorens, R. Ogaya, F. Lloret, P. Comas, M. Estiarte, and J. Terradas, 2004: Complex spatiotemporal phenological shifts as a response to rainfall changes. *New Phytologist*, **161**, 837-846.

Platnick, S., M. D. King, S. A. Ackerman, W. P. Menzel, B. A. Baum, J. C. Riédi, and R. A. Frey, 2003: The MODIS cloud products: Algorithms and examples from Terra. *IEEE Trans. Geosci. Remote Sens.*, **41**, 459-473.

Ramon, D. and R. Santer, 2005: Aerosol over land with MERIS, present and future. *Proceedings of the MERIS (A) ASTR Workshop (ESA SP-597).*

Reed, B. C., J. F. Brown, D. VanderZee, T. R. Loveland, J. W. Merchant, and D. O. Ohlen, 1994: Measuring phenological variability from satellite imagery. *J. Veg. Sci.*, **5**, 703-714.

Roy, D. P, P. Lewis, C. B. Schaaf, S. Devadiga, and L. Boschetti, 2006: The global impact of clouds on the production of MODIS bidirectional reflectance model-based composites for terrestrial monitoring. *IEEE Geosci. and Remote Sens. Letters*, **3(4)**, 452-456.

Schaaf, C. B., F. Gao, A. H. Strahler, W. Lucht, X. W. Li , T. Tsang, N. C. Strugnell, X. Y. Zhang, Y. F. Jin, J. P. Muller, P. Lewis, M. Barnsley, P. Hobson, M. Disney, G. Roberts, M. Dunderdale, C. Doll, R. P. d'Entremont, B. X. Hu, S. L. Liang, J. L. Privette, and D. Roy, 2002: First operational BRDF, albedo nadir reflectance products from MODIS. *Remote Sens. Environ.*, **83**, 135-148.

Schwartz, M. D., 1998: Green-wave phenology. *Nature*, **394**, 839-840.

____, and B. C. Reed, 1999: Surface phenology and satellite sensor-derived onset of greenness: An initial comparison. *Int. J. Remote Sens.*, **20**, 3451-3457.

Sellers, P. J., D. A. Randall, G. J. Collatz, J. A. Berry, C. B. Field, D. A. Dazlich, C. Zhang, and L. Bounoua, 1996: A revised land surface parameterization (SiB2) for atmospheric GCMs. Part 1: Model formulation. *J. Climate*, **9**, 676-705.

Tegen, I., B. Heinold, M. Todd, J. Helmert, R. Washington, and O. Dubovik, 2006: Modelling soil dust aerosol in the Bodele depressions during the BoDEx campaign. *Atmos. Chem. and Phys.*, **6**, 4345-4359.

Wang, K., J. Liu, X. Zhou, M. Sparrow, M. Ma, Z. Sun, and W. Jiang, 2004: Validation of the MODIS global albedo surface albedo product using ground measurements in a semidesert region on the Tibetan Plateau. *J. Geophys. Res.*, **109** (D5), doi:10.1029/2003JD004229.

Wen, G., A. Marshak, and R. F. Cahalan, 2006: Impact of 3-D clouds on clear-sky reflectance and aerosol retrieval in a biomass burning region of Brazil. *Geos. and Remote Sens. Letters*, **3**(1), 169-172.

White, M. A., P. E. Thornton, and S. W. Running, 1997: A continental phenology model for monitoring vegetation responses to interannual climatic variability. *Global Biogeochem. Cycles*, **11**, 217-234.

Whitlock, C. H., T. P. Charlock, W. F. Staylor, R. T. Pinker, I. Laszlo, A. Ohmura, H. Gilgen, T. Konzelman, R. C. DiPasquale, C. D. Moats, S. R. LeCroy, and N. A. Ritchey, 1995: First global WCRP shortwave surface radiation budget data set. *Bull. Amer. Meteor. Soc.*, **76**, 905-922.

Yu, H., Y. J. Kaufman, M. Chin, G. Feingold, L. A. Remer, T. L. Anderson, Y. Balkanski, N. Bellouin, O. Boucher, S. Christopher, P. DeCola, R. Kahn, D. Koch, N. Loeb, M. S. Reddy, M. Shulz, T. Takemura, and M. Zhou, 2005: A review of measurement-base assessments of the aerosol direct radiative effect and forcing. *Atmos. Chem. And Phys.*, **6**, 613-666.

Zhang, S., M. A. Friedl, C. B. Schaaf, A. H. Strahler, J. C. F. Hodges, F. Gao, and B. C. Reed, 2003: Monitoring vegetation phenology using MODIS. *Remote Sens. Environ.*, **84**, 471-475.

Zhang, Y., W. B. Rossow, and P. W. Stackhouse Jr., 2007: Comparison of different global information sources used in surface radiative flux calculation: Radiative properties of the surface. *J. Geophys. Res.*, **112**, doi:10.1029/2005JD007008.

FIGURE LEGENDS

Fig. 1. Number of high-quality flagged MOD43B3 retrievals preserved for each pixel in the spatially complete (a) five-year (2000-2004) aggregate climatology albedo data. For comparison, the difference between the climatology and single year data is shown in panels (b) through (f). Mid-latitude regions typically have more observations than areas of persistent clouds (tropics) or ephemeral and seasonal snow and low illumination angles (high latitudes). By definition, the aggregate product provides more complete temporal information than any single year of data.

Fig. 2. Temporal and spatial distribution of preserved high-quality flagged MOD43B3 retrievals and filled pixels at 0.86 μm for the 16-day periods of (a, b) January 1-16, (c, d) April 3-18, (e, f) July 12-27, and (g, h) September 30-October 14. Data from the five-year (2000-2004) climatology is presented in the left column (a, c, e, g), while the single-year 2000 albedo data is presented in the right column (b, d, f, h).

Fig. 3. Temporal and spatial distribution of preserved high-quality flagged MOD43B3 retrievals and filled pixels at 0.86 μm for the 16-day periods of (a, b) January 1-16, (c, d) April 3-18, (e, f) July 12-27, and (g, h) September 30-October 14. Single-year 2001 and 2002 data are presented in the left (a, c, e, g) and right (b, d, f, h) columns, respectively.

Fig. 4. Temporal and spatial distribution of preserved high-quality flagged MOD43B3 retrievals and filled pixels at 0.86 μm for the 16-day periods of (a, b) January 1-16, (c, d) April 3-18, (e, f) July 12-27, and (g, h) September 30-October 14. Single-year 2003 and 2004 data are presented in the left (a, c, e, g) and right (b, d, f, h) columns, respectively.

Fig. 5. Spatially complete diffuse bihemispherical (white-sky) albedo at 0.86 μm

for the 16-day periods of (a, b) January 1-16, (c, d) April 3-18, (e, f) July 12-27, and (g, h) September 30-October 14. Data from the five-year (2000-2004) climatology is presented in the left column (a, c, e, g), while the difference in the single-year 2000 albedo data, compared to the climatology, is presented in the right column (b, d, f, h).

Fig. 6. Spatially complete diffuse bihemispherical (white-sky) albedo at 0.86 μm for the 16-day periods of (a, b) January 1-16, (c, d) April 3-18, (e, f) July 12-27, and (g, h) September 30-October 14. Departures in albedo from the five-year (2000-2004) climatology for single-year 2001 (left column, a, c, e, g), and 2002 (right column, b, d, f, h) albedo data are presented.

Fig. 7. Spatially complete diffuse bihemispherical (white-sky) albedo at 0.86 μm for the 16-day periods of (a, b) January 1-16, (c, d) April 3-18, (e, f) July 12-27, and (g, h) September 30-October 14. Departures in albedo from the five-year (2000-2004) climatology for single-year 2003 (left column, a, c, e, g), and 2004 (right column, b, d, f, h) albedo data are presented

Fig. 8. Mean diffuse bihemispherical (white-sky) albedo values computed by 10° latitude belts for three bands (0.47 and 0.86 μm narrowband, and the 0.3-5.0 μm shortwave broadband) during the 16-day period of July 12-27 (data day 193). Trends are computed for three ecosystem classes, cropland (a and b), grassland (c and d), and mixed forest (e and f) from the five-year aggregate climatology (a, c, and e) and the 2002 single-year albedo data (b, d, and f).

Fig. 9. Mean diffuse bihemispherical (white-sky) albedo values computed for each 16-day period for three bands (0.47 and 0.86 μm narrowband, and the 0.3-5.0 μm shortwave broadband) over the 50°N-40°N latitude belt. Trends are computed for three ecosystem classes, cropland (a and b),

grassland (c and d), and mixed forest (e and f) from the five-year aggregate climatology (a, c, and e) and the 2002 single-year albedo data (b, d, and f).

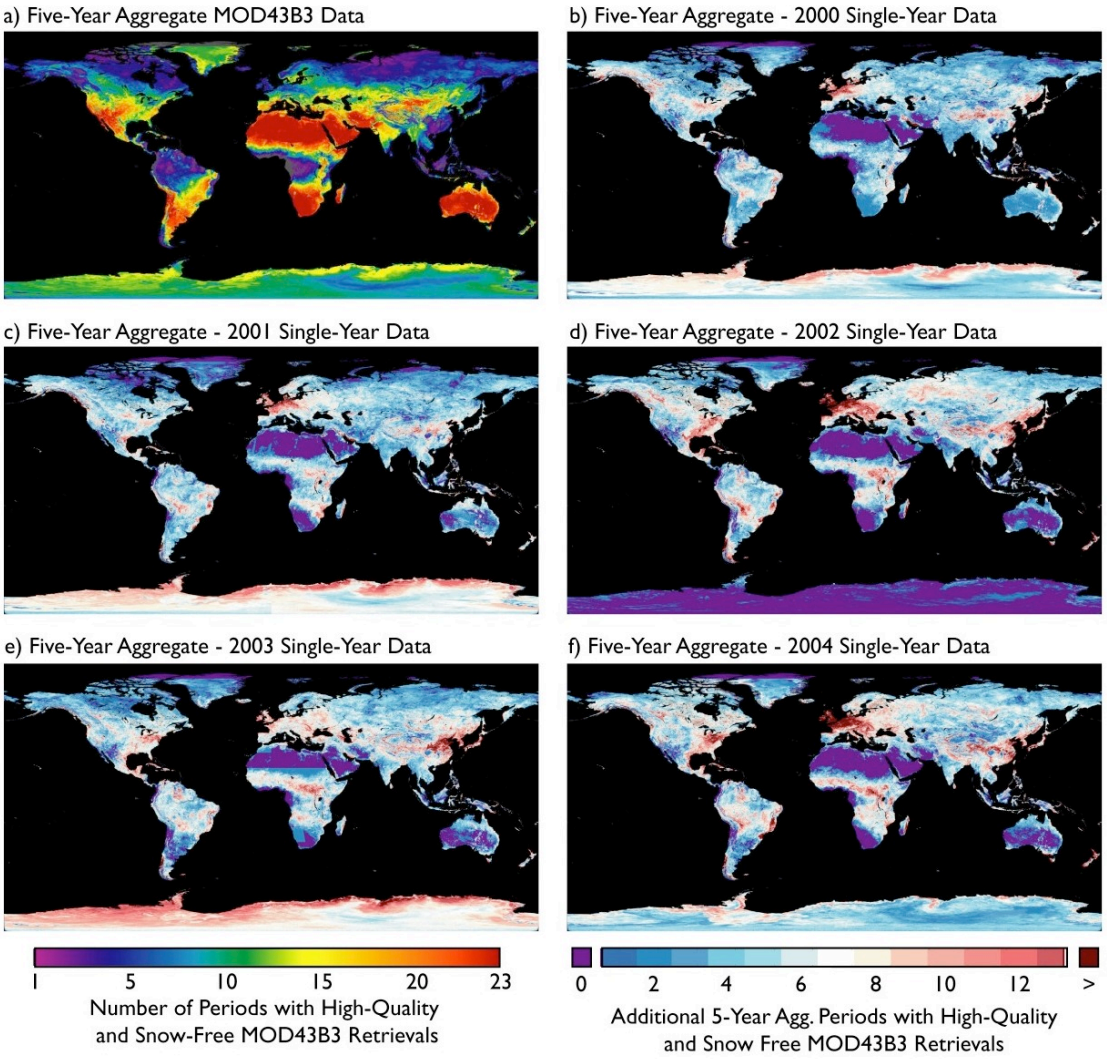

Fig. 1. Number of high-quality flagged MOD43B3 retrievals preserved for each pixel in the spatially complete (a) five-year (2000-2004) aggregate climatology albedo data. For comparison, the difference between the climatology and single year data is shown in panels (b) through (f). Mid-latitude regions typically have more observations than areas of persistent clouds (tropics) or ephemeral and seasonal snow and low illumination angles (high latitudes). By definition, the aggregate product provides more complete temporal information than any single year of data.

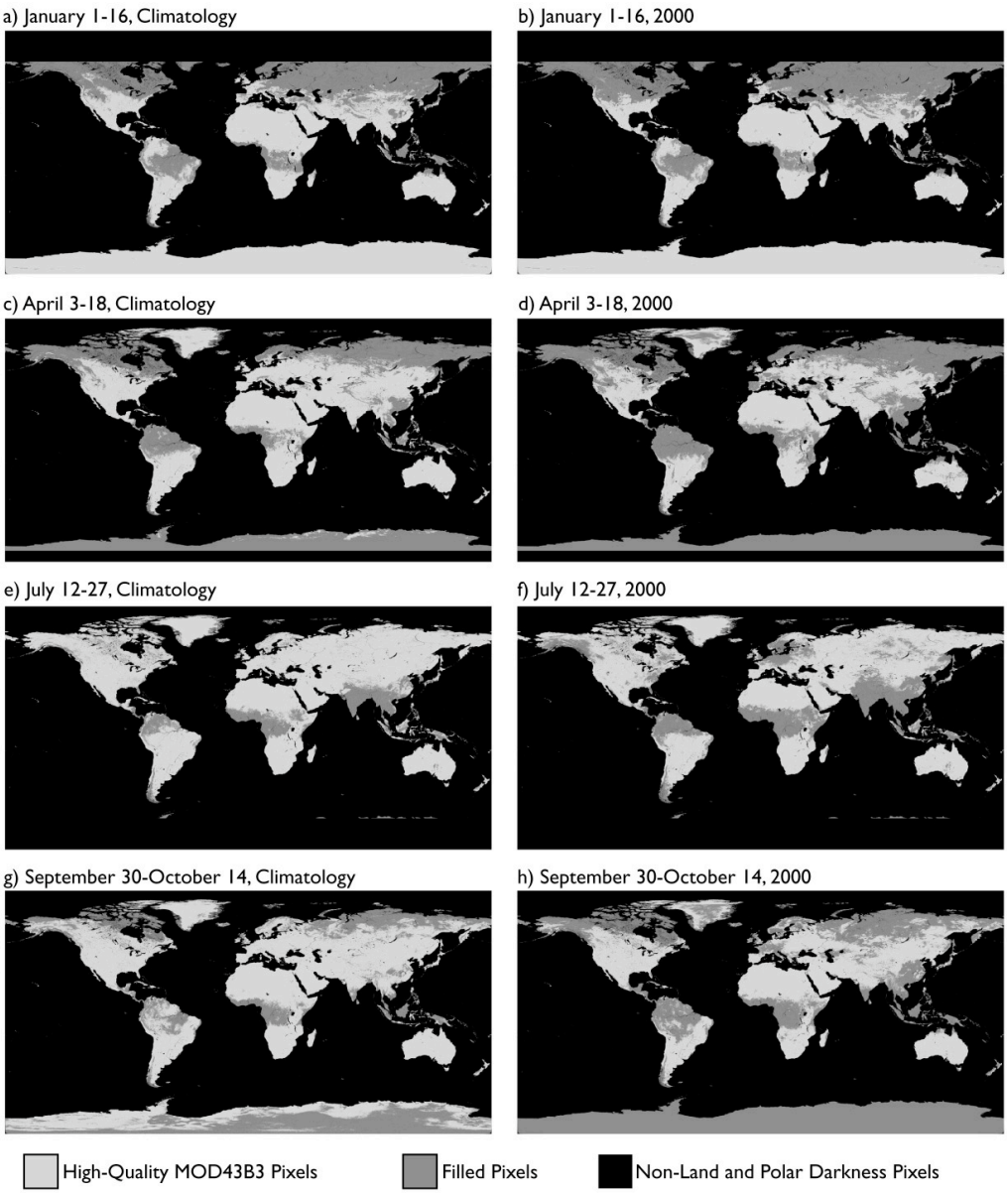

Fig. 2. Temporal and spatial distribution of preserved high-quality flagged MOD43B3 retrievals and filled pixels at 0.86 μm for the 16-day periods of (a, b) January 1-16, (c, d) April 3-18, (e, f) July 12-27, and (g, h) September 30-October 14. Data from the five-year (2000-2004) climatology is presented in the left column (a, c, e, g), while the single-year 2000 albedo data is presented in the right column (b, d, f, h).

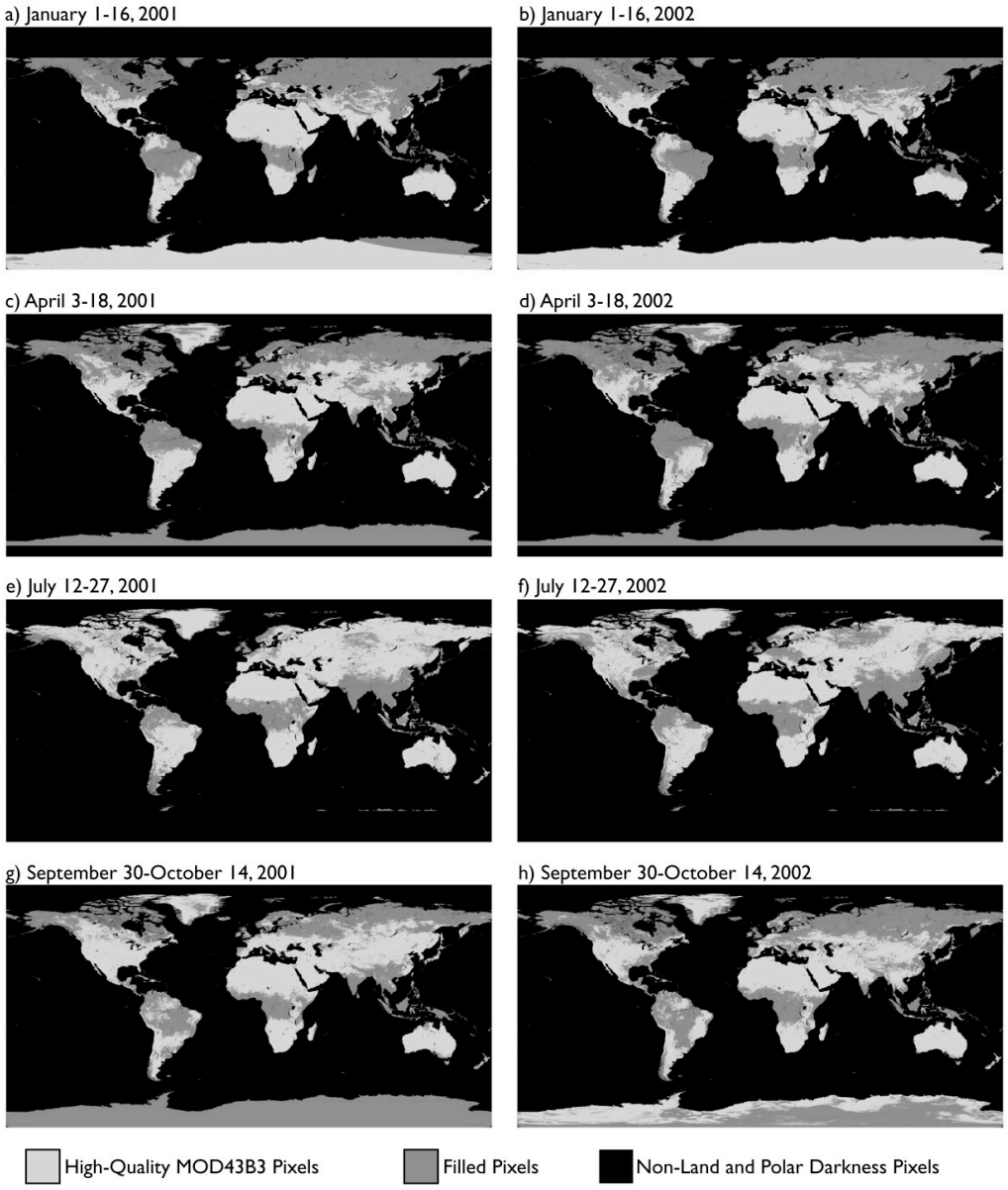

Fig. 3. Temporal and spatial distribution of preserved high-quality flagged MOD43B3 retrievals and filled pixels at 0.86 μm for the 16-day periods of (a, b) January 1-16, (c, d) April 3-18, (e, f) July 12-27, and (g, h) September 30-October 14. Single-year 2001 and 2002 data are presented in the left (a, c, e, g) and right (b, d, f, h) columns, respectively.

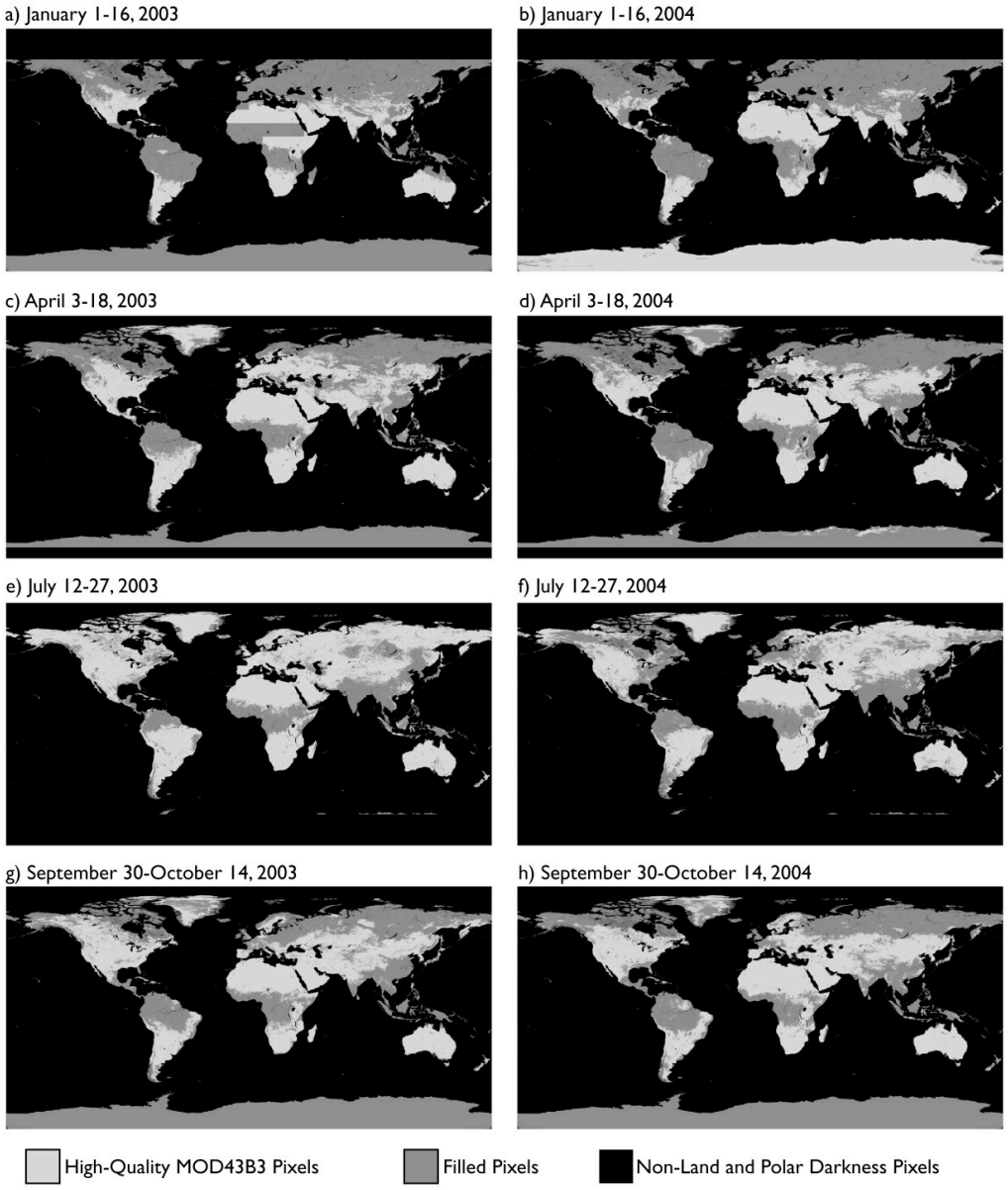

Fig. 4. Temporal and spatial distribution of preserved high-quality flagged MOD43B3 retrievals and filled pixels at 0.86 μm for the 16-day periods of (a, b) January 1-16, (c, d) April 3-18, (e, f) July 12-27, and (g, h) September 30-October 14. Single-year 2003 and 2004 data are presented in the left (a, c, e, g) and right (b, d, f, h) columns, respectively.

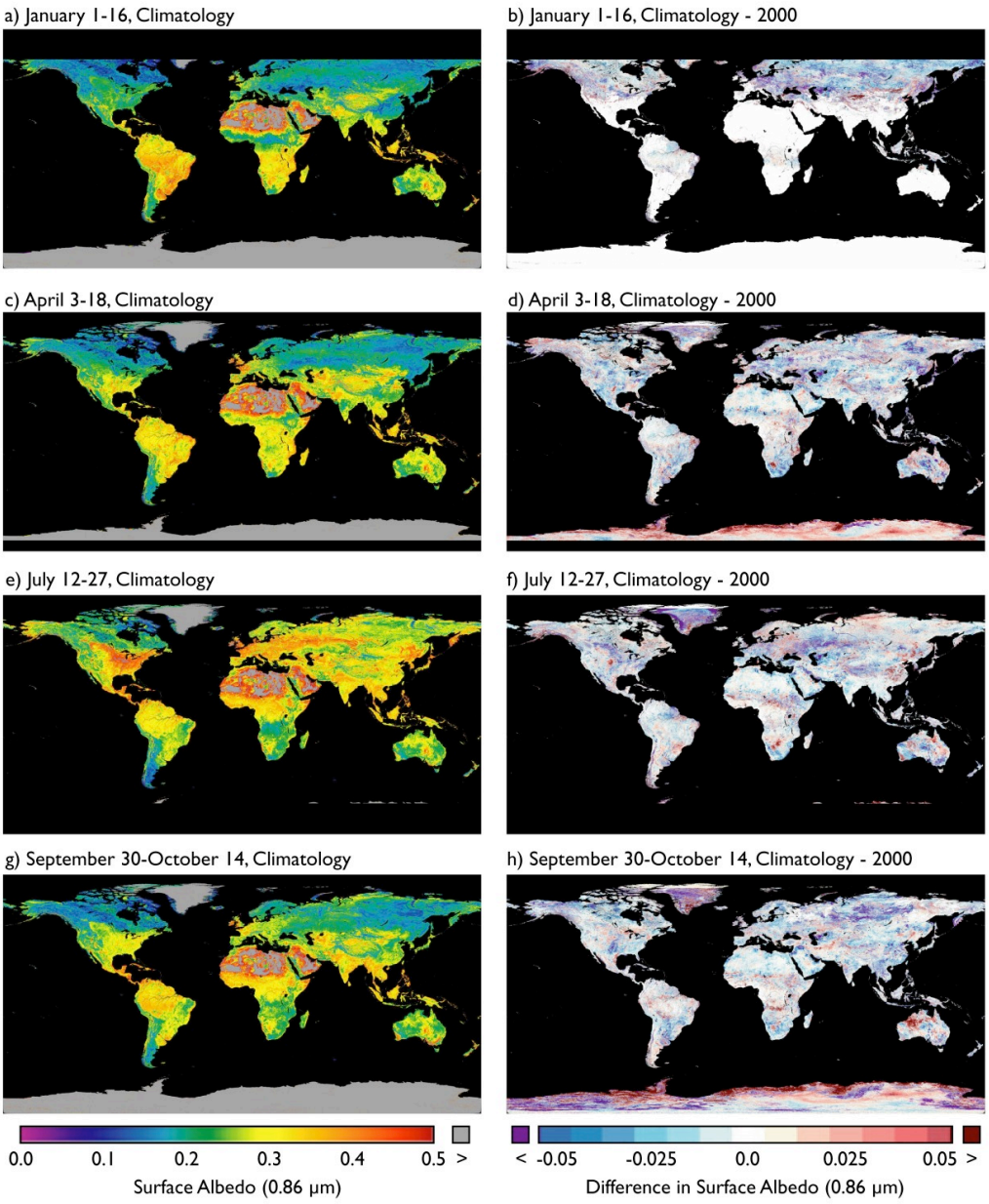

Fig. 5. Spatially complete diffuse bihemispherical (white-sky) albedo at 0.86 μm for the 16-day periods of (a, b) January 1-16, (c, d) April 3-18, (e, f) July 12-27, and (g, h) September 30-October 14. Data from the five-year (2000-2004) climatology is presented in the left column (a, c, e, g), while the difference in the single-year 2000 albedo data, compared to the climatology, is presented in the right column (b, d, f, h).

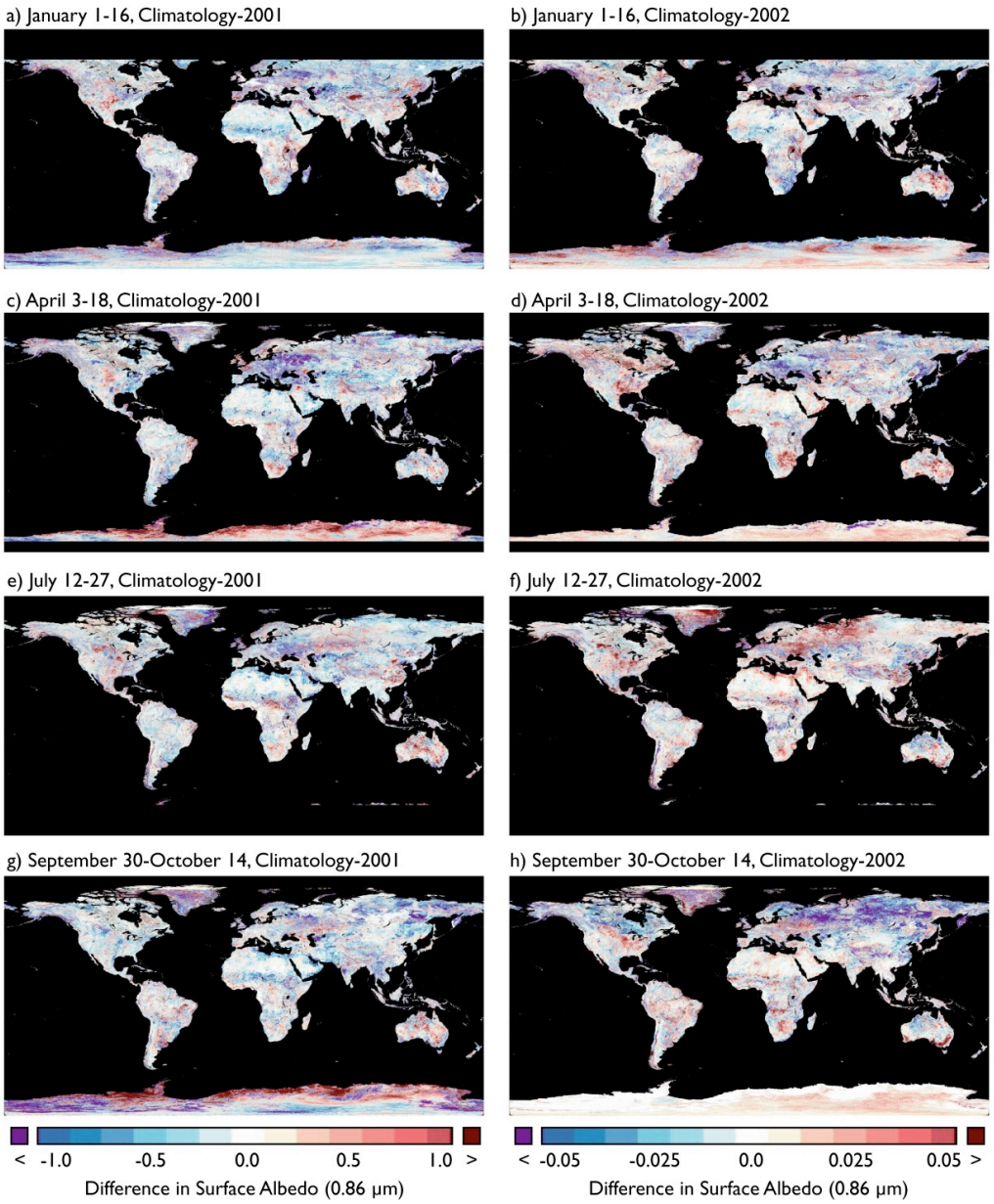

Fig. 6. Spatially complete diffuse bihemispherical (white-sky) albedo at 0.86 μm for the 16-day periods of (a, b) January 1-16, (c, d) April 3-18, (e, f) July 12-27, and (g, h) September 30-October 14. Departures in albedo from the five-year (2000-2004) climatology for single-year 2001 (left column, a, c, e, g), and 2002 (right column, b, d, f, h) albedo data are presented.

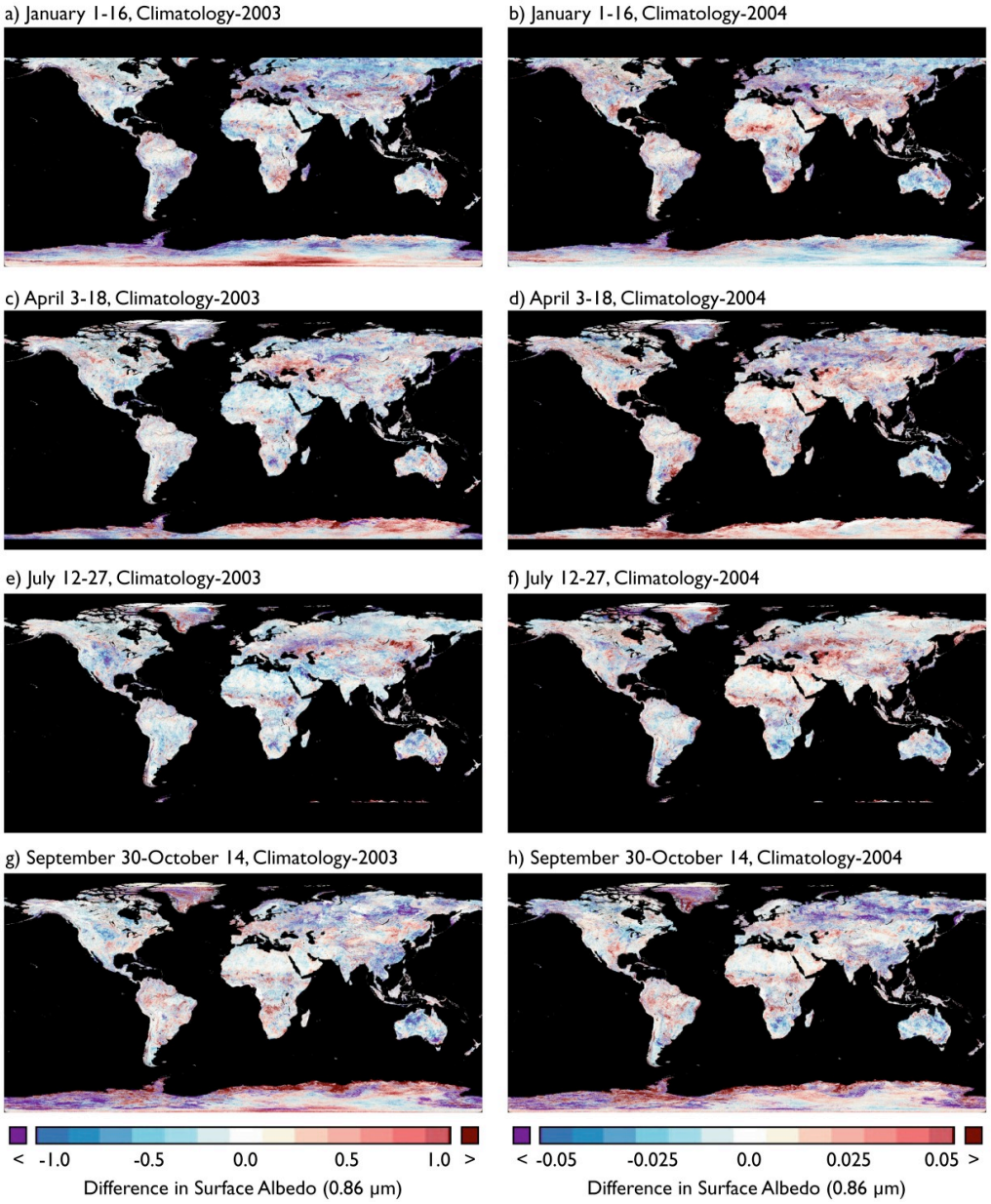

Fig. 7. Spatially complete diffuse bihemispherical (white-sky) albedo at 0.86 μm for the 16-day periods of (a, b) January 1-16, (c, d) April 3-18, (e, f) July 12-27, and (g, h) September 30-October 14. Departures in albedo from the five-year (2000-2004) climatology for single-year 2003 (left column, a, c, e, g), and 2004 (right column, b, d, f, h) albedo data are presented.

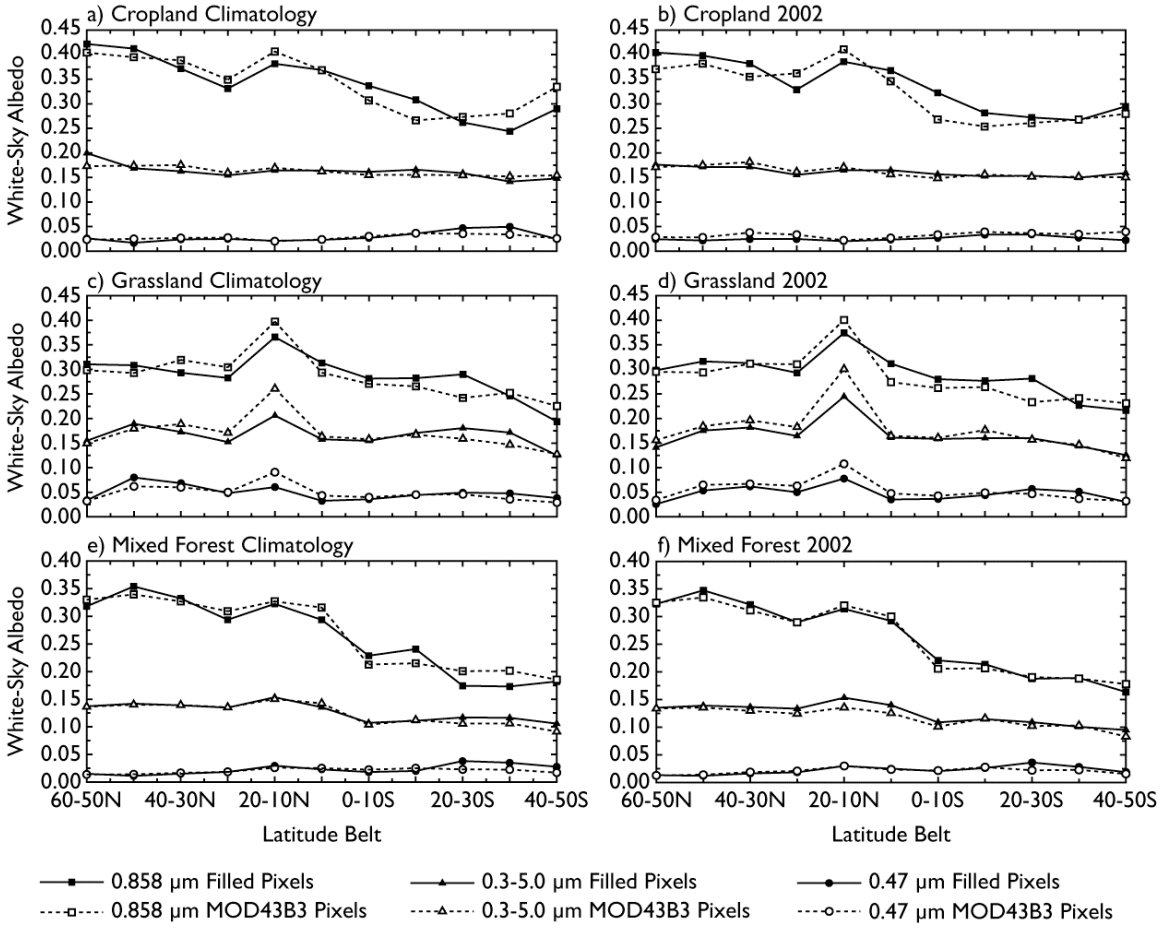

Fig. 8. Mean diffuse bihemispherical (white-sky) albedo values computed by 10° latitude belts for three bands (0.47 and 0.86 μm narrowband, and the 0.3-5.0 μm shortwave broadband) during the 16-day period of July 12-27 (data day 193). Trends are computed for three ecosystem classes, cropland (a and b), grassland (c and d), and mixed forest (e and f) from the five-year aggregate climatology (a, c, and e) and the 2002 single-year albedo data (b, d, and f).

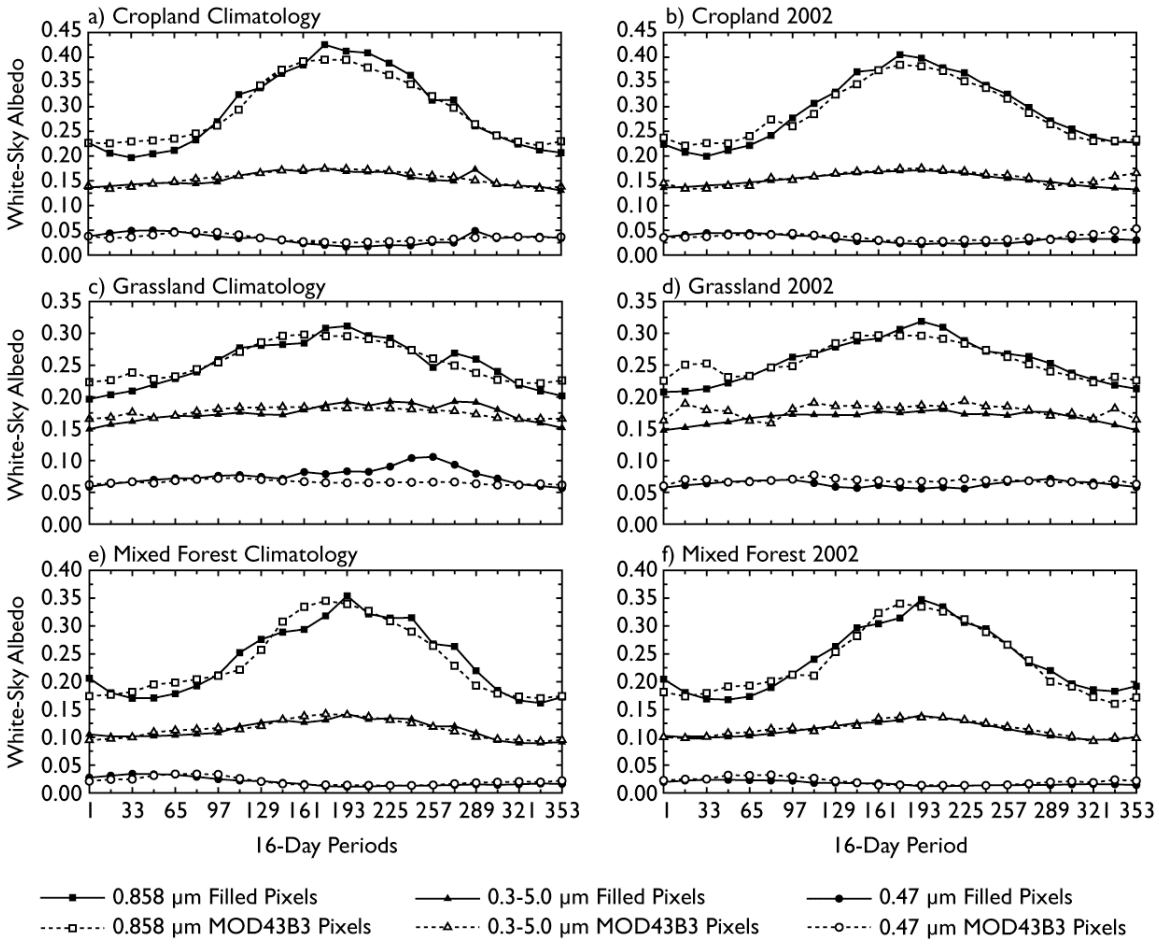

Fig. 9. Mean diffuse bihemispherical (white-sky) albedo values computed for each 16-day period for three bands (0.47 and 0.86 μm narrowband, and the 0.3-5.0 μm shortwave broadband) over the 50°N-40°N latitude belt. Trends are computed for three ecosystem classes, cropland (a and b), grassland (c and d), and mixed forest (e and f) from the five-year aggregate climatology (a, c, and e) and the 2002 single-year albedo data (b, d, and f).